

# QCD radiative corrections to $\chi_{cJ}$ production at hadron colliders

Yan-Qing Ma <sup>(a)</sup>, Kai Wang <sup>(a)</sup>, and Kuang-Ta Chao <sup>(a,b)</sup>

(a) Department of Physics and State Key Laboratory of Nuclear Physics and Technology, Peking University, Beijing 100871, China

(b) Center for High Energy Physics, Peking University, Beijing 100871, China

To clarify the outstanding problem in charmonium production that existing theories cannot explain the observed cross sections of  $\chi_{cJ}$  ( $J = 0, 1, 2$ ) and ratio  $R_{\chi_c} = \sigma_{\chi_{c2}}/\sigma_{\chi_{c1}} \approx 0.75$  (in contrast to the spin counting value  $5/3$ ) at the Tevatron, we study the complete next-to-leading order radiative corrections in nonrelativistic QCD, and find next-to-leading order contributions of  ${}^3P_J^{[1]}$  are more important than leading order at high  $p_T$ , and  ${}^3P_1^{[1]}$  decreases slower than  ${}^3P_2^{[1]}$ , implying a natural explanation for the  $R_{\chi_c}$  puzzle. By fitting  $R_{\chi_c}$ , the predicted cross sections of  $\chi_{cJ}$  are found to agree with data. The result indicates color-octet contribution is crucially needed, thus providing a unique test for heavy quarkonium production mechanisms. Feed-down contributions of  $\chi_{cJ}$  to prompt  $J/\psi$  production are estimated to be substantial, about  $30 - 40\%$  at  $p_T = 20$  GeV. Production of  $\chi_{cJ}$  ( $J=0,1,2$ ) at the LHC is also predicted.

PACS numbers: 12.38.Bx, 13.25.Gv, 14.40.Pq

Heavy quarkonium production remains a challenging problem in understanding quantum chromodynamics. Among others, the puzzle of  $J/\psi(\psi')$  production cross sections and polarizations at large transverse momentum  $p_T$  at the Tevatron is crucial in testing the color-octet (CO) and color-singlet (CS) mechanisms in NRQCD[1] and other mechanisms (for reviews see e.g.[2]). The P-wave charmonia  $\chi_{cJ}$  production is equally important, since they give substantial feed-down contributions to the prompt  $J/\psi$  production through decays  $\chi_{cJ} \rightarrow \gamma J/\psi$ . An even more important issue in  $\chi_{cJ}$  production concerns the ratio of production rates of  $\chi_{c2}$  to  $\chi_{c1}$ .

The CDF Collaboration measured the ratio

$$R_{\chi_c} = \sigma_{\chi_{c2}}/\sigma_{\chi_{c1}} \quad (1)$$

to be about 0.75 for  $p_T > 4$  GeV, and even smaller when  $p_T$  becomes larger[3]. But at leading order (LO) in  $\alpha_s$ , NRQCD predicts the  $\chi_c$  production cross sections to scale as  $1/p_T^6$  in the CS  ${}^3P_J^{[1]}$  channels yet scale as  $1/p_T^4$  in the CO  ${}^3S_1^{[8]}$  channel. Thus  ${}^3S_1^{[8]}$  would dominate at large  $p_T$ , predicting the ratio to be  $5/3$  by spin counting[4, 5], which is much larger than the measured value 0.75. Meanwhile, the color-evaporation model (CEM) predicts the ratio to be always  $5/3$  in all orders of  $\alpha_s$  simply based on spin counting. It seems as if no existing theory agrees with the measured  $R_{\chi_c}$ . However, there could be a good chance for NRQCD to explain this puzzle, because the next-to-leading order (NLO) contributions in  $\alpha_s$  will change the large  $p_T$  behavior of cross sections. In particular, contributions of CS  ${}^3P_J^{[1]}$  channels scale as  $1/p_T^4$  at NLO, more important than  $1/p_T^6$  at LO. So it is necessary to study  $\chi_{cJ}$  production at NLO to see how the value of  $R_{\chi_c}$  can be changed at large  $p_T$ .

Another issue concerns the CO mechanism, which has been studied extensively in S-wave charmonium  $J/\psi$  production. Large discrepancies between experiments and

LO predictions[6] for  $J/\psi$  exclusive and inclusive production in  $e^+e^-$  annihilation at  $B$  factories can be resolved at NLO within CS channels[7]. For  $J/\psi$  photoproduction at HERA, complete calculations[8] slightly favor the presence of CO contributions. For  $J/\psi$  production at the Tevatron, the NLO correction in CS channels enhances the cross section at large  $p_T$  by 2 orders of magnitude [9, 10] and reduces the discrepancies between theory and experiment. So, a crucial issue in charmonium production is whether the CO contributions are still needed. To clarify this, we must go beyond S-wave and study P-wave quarkonia, e.g.,  $\chi_{cJ}$  production.

In view of the urgency, we study the NLO QCD corrections to  $\chi_{cJ}$  hadroproduction in this work. Within NRQCD factorization, the inclusive cross section for the direct  $\chi_{cJ}$  production in hadron-hadron collisions reads

$$\begin{aligned} d\sigma[pp \rightarrow \chi_{cJ} + X] &= \sum_n d\hat{\sigma}[(c\bar{c})_n] \frac{\langle \mathcal{O}_n^{\chi_{cJ}} \rangle}{m_c^{2L_n}} \\ &= \sum_{i,j,n} \int dx_1 dx_2 G_{i/p} G_{j/p} \times d\hat{\sigma}[i + j \rightarrow (c\bar{c})_n + X] \langle \mathcal{O}_n^{\chi_{cJ}} \rangle, \end{aligned} \quad (2)$$

where  $p$  is either a proton or an antiproton, the indices  $i, j$  run over all the partonic species and  $n$  denotes the color, spin and angular momentum ( $L_n$ ) of the intermediate  $c\bar{c}$  pair. In this work, we calculate the cross sections at NLO in  $\alpha_s$  and LO in  $v$  (the relative velocity of quark and antiquark). So only two channels  ${}^3P_J^{[1]}$  and  ${}^3S_1^{[8]}$  in the present calculation are involved. The long-distance-matrix elements (LDMEs)  $\langle \mathcal{O}_n^{\chi_{cJ}} \rangle$  are related to the transition probabilities from the intermediate state  $(c\bar{c})_n$  into  $\chi_{cJ}$ , and are governed by the nonperturbative QCD dynamics. Note that our definition of CS LDME  $\langle \mathcal{O}_n^{\chi_{cJ}}({}^3P_J^{[1]}) \rangle$  is different from that in Ref.[1] by a factor of  $1/(2N_c)$ . And  $\langle \mathcal{O}_n^{\chi_{cJ}}({}^3P_J^{[1]}) \rangle$  ( $J=0,1,2$ ) are related to just one matrix element by spin symmetry.

We use FeynArts[12] to generate Feynman diagrams

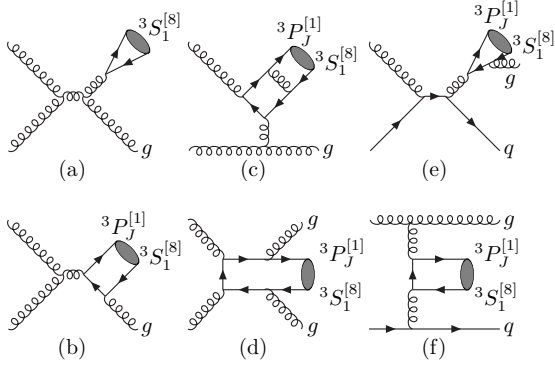


FIG. 1: Representative Feynman diagrams for  $\chi_{cJ}$  hadroproduction at LO and NLO. The gluon-gluon and gluon-quark subprocesses are all included. In (b)-(f) both color-singlet  ${}^3P_J^{[1]}$  and color-octet  ${}^3S_1^{[8]}$  channels contribute.

and amplitudes. Some representative diagrams are shown in Fig. 1. There are generally ultraviolet (UV), infrared (IR) and Coulomb singularities. Conventional dimensional regularization (CDR) with  $D = 4 - 2\epsilon$  is adopted to regularize them. We have checked analytically that all singularities are canceled exactly.

The UV divergences from self-energy and triangle diagrams are removed by renormalization. The renormalization constants  $Z_m$ ,  $Z_2$ ,  $Z_{2l}$  and  $Z_3$ , which correspond, respectively, to the charm quark mass  $m_c$ , charm-field  $\psi_c$ , light quark field  $\psi_q$  and gluon field  $A_\mu^a$  are defined in the on-mass-shell(OS) scheme, while  $Z_g$  corresponding to the QCD gauge coupling  $\alpha_s$  is defined in the modified-minimal-subtraction( $\overline{\text{MS}}$ ) scheme:

$$\begin{aligned} \delta Z_m^{OS} &= -3C_F \frac{\alpha_s}{4\pi} N_\epsilon \left[ \frac{1}{\epsilon_{UV}} + \frac{4}{3} \right], \\ \delta Z_2^{OS} &= -C_F \frac{\alpha_s}{4\pi} N_\epsilon \left[ \frac{1}{\epsilon_{UV}} + \frac{2}{\epsilon_{IR}} + 4 \right], \\ \delta Z_{2l}^{OS} &= -C_F \frac{\alpha_s}{4\pi} N_\epsilon \left[ \frac{1}{\epsilon_{UV}} - \frac{1}{\epsilon_{IR}} \right], \\ \delta Z_3^{OS} &= \frac{\alpha_s}{4\pi} N_\epsilon \left[ (\beta_0(n_f) - 2C_A) \left( \frac{1}{\epsilon_{UV}} - \frac{1}{\epsilon_{IR}} \right) \right], \\ \delta Z_g^{\overline{\text{MS}}} &= -\frac{\beta_0(n_f)}{2} \frac{\alpha_s}{4\pi} N_\epsilon \left[ \frac{1}{\epsilon_{UV}} + \ln \frac{m_c^2}{\mu_r^2} \right], \end{aligned} \quad (3)$$

where  $N_\epsilon = \left( \frac{4\pi\mu_r^2}{m_c^2} \right)^\epsilon \Gamma(1 + \epsilon)$  is a overall factor in our calculation,  $\beta_0(n_f) = \frac{11}{3}C_A - \frac{4}{3}T_F n_f$  is the one-loop coefficient of the QCD beta function,  $n_f = 3$  is the number of active quark flavors and  $\mu_r$  is the renormalization scale.

IR singularities arising from loop integration and phase space integration of the real correction partially cancel each other. The remaining singularities of the S-wave state  ${}^3S_1^{[8]}$  are absorbed by the proton parton-distribution-functions (PDFs), while that of  ${}^3P_J^{[1]}$  states are absorbed by both the proton PDFs and  $\langle \mathcal{O}^{\chi_{c0}}({}^3S_1^{[8]}) \rangle$ . We extract poles in the real corrections using the phase

space slicing method[13]. We note that to correctly get the soft poles, the eikonal current should be taken before the heavy quarks are coupled to states with definite quantum numbers. We verify that our results are independent of the two cuts introduced in the phase space slicing for each subgroup associated with a real correction process.

There are thousands of diagrams which are handled by our self-written **Mathematica** program and then changed into **C++** code to perform convolution and phase space integration. To perform the calculation, two different methods are used, resulting in two independent computer codes. In one of our methods, the virtual corrections are calculated numerically and using **QCDLoop**[14] to separate the singularities and finite result, while the real corrections are calculated using the helicity method. In the second method, we expand the singularities analytically and use **LoopTools**[15] to get the finite result, while the real corrections are calculated by directly squaring the amplitudes. Results of the two methods are found to coincide with each other.

Essentially, in our calculation the most complicated part is the loop-correction for P-wave channels, where the derivation of the amplitude with respect to the relative momentum of heavy quarks  $Q$  and  $\bar{Q}$  is involved. This derivation is equivalent to having one additional massive vector boson in the calculation, which causes complicated tensor loop integrals and entangled pattern of infrared (IR) singularities. Based on the formula in Ref.[11], we developed a new method to perform NLO corrections for processes involving bound states. This method makes the calculation of P-wave heavy quarkonium hadroproduction at NLO become possible. The details of our method will be presented elsewhere[16].

Thanks to the LHAPDF interface[17], the CTEQ6L1 and CTEQ6M PDFs are used for LO and NLO calculations respectively. The charm quark mass is set to be  $m_c = 1.5$  GeV, while the renormalization, factorization, and NRQCD scales are  $\mu_r = \mu_f = m_T$  and  $\mu_\Lambda = m_c$ , where  $m_T = \sqrt{p_T^2 + 4m_c^2}$  is the  $\chi_{cJ}$  transverse mass. The center-of-mass energies  $\sqrt{S}$  are 1.96 TeV at the Tevatron RUN II and 14 TeV at the LHC. To estimate theoretical uncertainties, we vary  $\mu_r$  and  $\mu_f$  from  $m_T/2$  to  $2m_T$  and choose  $m_c = 1.5 \pm 0.1$  GeV. Note that there exists a large cancellation for errors between fitting data and predictions. Thus to avoid double counting, our strategy is to consider all errors in the fit procedure and include them in fitted parameters, while when predicting new quantities, we just consider errors due to fitted parameters.

We begin our numerical analysis by comparing the short-distance coefficients  $\hat{\sigma}[{}^3P_J^{[1]}]$  of the  ${}^3P_J^{[1]}$  channels and  $\hat{\sigma}[{}^3S_1^{[8]}]$  of the  ${}^3S_1^{[8]}$  channel at NLO. We find that at NLO the most significant change is the large  $p_T$  behavior in the  ${}^3P_J^{[1]}$  channels: it scales as  $1/p_T^4$  at large  $p_T$  at NLO, in contrast to  $1/p_T^6$  at LO. As shown in Fig. 2, at LO the  ${}^3P_J^{[1]}$  channels are negligible at high  $p_T$ , whereas

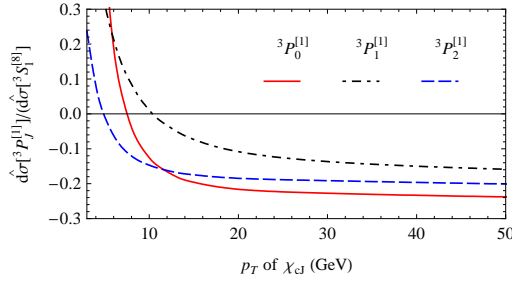


FIG. 2: The ratio of  $d\hat{\sigma}[3P_J^{[1]}]$  to  $d\hat{\sigma}[3S_1^{[8]}]$  at NLO as a function of  $p_T$  at the Tevatron. The cut  $|y_{\chi_{cJ}}| < 1$  is chosen to compare with the CDF data of Ref. [3].

at NLO the  $3P_J^{[1]}$  channels are comparable to the  $3S_1^{[8]}$  channel even at  $p_T \approx 50$  GeV. Another important but unique feature is that the  $3P_J^{[1]}$  channels give large values at high  $p_T$ , but surprisingly with negative signs. We note that the negative values are not caused by the choice of  $\mu_\Lambda$ , though this may affect their absolute values. In fact, detailed investigation reveals that the negative values are originated from the renormalization scheme (RS) for the NRQCD LDMEs  $\langle \mathcal{O}_{\chi_{c0}}(3S_1^{[8]}) \rangle$ . The RS in this work is the conventional  $\overline{\text{MS}}$  scheme. One may use another RS to get different values of  $d\hat{\sigma}[3P_J^{[1]}]$ , but this should not change the physical result, because the RS dependence of short-distance coefficients of  $3P_J^{[1]}$  are canceled by the RS dependence of  $\langle \mathcal{O}_{\chi_{c0}}(3S_1^{[8]}) \rangle$ , and the final physical results are independent of the choice of it. Especially,  $d\sigma[\chi_{cJ}]$  and  $R_{\chi_c}$  are independent of the RS and  $\mu_\Lambda$ , and their values should always be positive.

From Fig. 2 we see that the  $3P_1^{[1]}$  channel decreases slower than the  $3P_2^{[1]}$  channel. Considering also that  $3P_J^{[1]}$  channels are comparable to the  $3S_1^{[8]}$  channel at high  $p_T$ , we may naturally explain the CDF data[3] that the production rate of  $\chi_{c1}$  exceeds that of  $\chi_{c2}$  at high  $p_T$ . We define the ratio

$$r = \frac{\langle \mathcal{O}_{\chi_{c0}}(3S_1^{[8]}) \rangle}{\langle \mathcal{O}_{\chi_{c0}}(3P_J^{[1]}) \rangle / m_c^2} \Big|_{\overline{\text{MS}}, \mu_\Lambda = m_c}. \quad (4)$$

The bound of  $r > 0.24$  is needed to get a positive production rate of  $\chi_{c0}$  at high  $p_T$ , as shown in Fig. 2. With this definition, we can give an asymptotic expression of  $R_{\chi_c}$  at the Tevatron with  $|y_{\chi_{cJ}}| < 1$ :

$$R_{\chi_c} = \frac{5 r d\hat{\sigma}[3S_1^{[8]}] + d\hat{\sigma}[3P_2^{[1]}]}{3 r d\hat{\sigma}[3S_1^{[8]}] + d\hat{\sigma}[3P_1^{[1]}]} \rightarrow \frac{5 r - 0.20}{3 r - 0.16}, \quad (5)$$

where the numbers  $-0.20$  and  $-0.16$  can be read from Fig. 2. Because of these two numbers,  $R_{\chi_c}$  must be smaller than  $5/3$  at high  $p_T$ . By fitting the data [3], we get  $r = 0.27_{-0.01-0.04-0.04}^{+0.01+0.05+0.04} \approx 0.27 \pm 0.06$ , where the errors come from data, scale dependence and  $m_c$  dependence respectively. In the fitting procedure, the mass

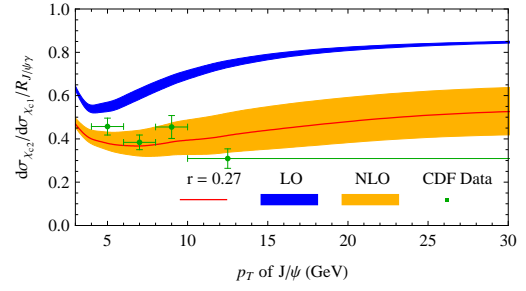


FIG. 3: Transverse momentum distribution of ratio  $R_{\chi_c}/R_{J/\psi\gamma}$  at the Tevatron with cut  $|y_{\chi_{cJ}}| < 1$ . The CDF data is taken from Ref.[3]. The lower and upper bounds of LO and NLO are constrained by  $0.24 < r < 0.33$ .

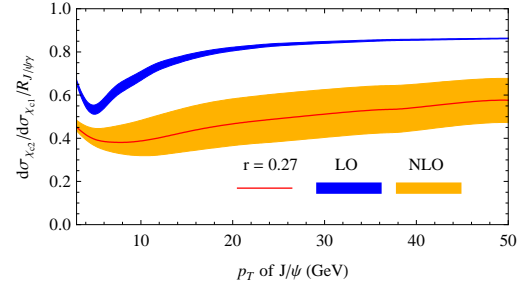


FIG. 4: The same as Fig. 3 but for LHC with cut  $|y_{\chi_{cJ}}| < 3$ .

difference between  $\chi_{cJ}$  and  $J/\psi$  is also considered. It can be found that the value of  $r$  is compatible with the naive velocity scaling rule  $r \approx O(1)$  [1].

As shown in Fig. 3, the NLO predictions present a much better compatibility with data than LO, where  $r$  is constrained by  $0.24 < r < 0.33$  and  $R_{J/\psi\gamma} \equiv \mathcal{B}(\chi_{c1} \rightarrow J/\psi\gamma)/\mathcal{B}(\chi_{c2} \rightarrow J/\psi\gamma) = 1.91$  as in Ref.[3]. In Fig. 4, we show predictions for  $R_{\chi_c}$  at the LHC. Note that, the ratio  $R_{\chi_c}$  is sensitive to  $r$  at NLO. Thus measurement of  $R_{\chi_c}$  at high  $p_T$  will give a strict constraint on  $r$ .

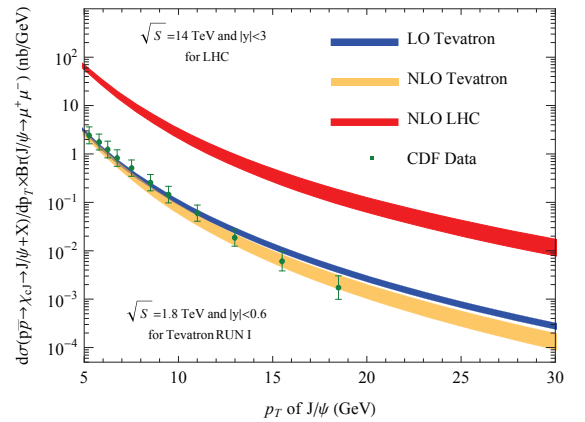


FIG. 5: Transverse momentum distribution of  $\chi_{cJ}$  feed down to  $J/\psi$  at the Tevatron RUN I and LHC, where RUN I data is taken from Ref.[19].

To predict the production cross sections, we still need a CS matrix element  $\langle \mathcal{O}^{\chi_{c0}}(P_J^{[1]}) \rangle$ . As a widely adopted choice, we take the potential model result  $|R'_P(0)|^2 = 0.075 \text{ GeV}^5$  (see the B-T model in [18]) as our input parameter. Then we compare our prediction for  $\chi_{cJ}$  production at the Tevatron with RUN I data in Fig. 5, where  $\sqrt{S} = 1.8 \text{ TeV}$  and  $|y_{\chi_{cJ}}| < 0.6$ . Because of a large negative correction for CS channel at large  $p_T$ , NLO results decrease faster than LO, and give a more reasonable interpretation for experimental data. The differences between  $\chi_{cJ}$  production at the Tevatron RUN II with  $\sqrt{S} = 1.96 \text{ TeV}$  and that of RUN I are within a factor of 20 percent for all  $p_T$  region, so we do not present them here. At the Tevatron, the feed-down contribution from  $\chi_{cJ}$  has a rather large proportion of the total  $J/\psi$  production cross section. If we choose  $r = 0.24(0.27)$ , the proportion is 25(30)% at  $p_T = 10 \text{ GeV}$ , and reaches to about 30(40)% at  $p_T = 20 \text{ GeV}$ . Because of this large proportion,  $\chi_{cJ}$  feed-down will have an important effect on  $J/\psi$  polarization in  $J/\psi$  prompt production, and should be further clarified when dealing with the  $J/\psi$  polarization puzzle. The prediction for  $\chi_{cJ}$  production at the LHC is also presented in Fig. 5, where  $\sqrt{S} = 14 \text{ TeV}$  and  $|y_{\chi_{cJ}}| < 3$ .

In summary, we calculate NLO QCD corrections to  $\chi_{cJ}$  production at the Tevatron and LHC, including both CS and CO channels. We find  $^3P_J^{[1]}$  channels give large contributions at high  $p_T$  and  $^3P_1^{[1]}$  decreases slower than  $^3P_2^{[1]}$ , then the measured ratio of  $R_{\chi_c}$  at the Tevatron can

be naturally explained. Moreover, our result shows that the measured  $R_{\chi_c}$  disfavors CEM, but favors NRQCD. By fitting the observed ratio  $R_{\chi_c}$ , we extract the ratio of CO to CS matrix element to be  $r = 0.27_{-0.03}^{+0.06}$ , which is used to predict the production rates of  $\chi_{cJ}$  at the Tevatron RUN I and leads to a good agreement with data. As a result, for the first time, the observed rates of  $\chi_{cJ}$  and ratio  $R_{\chi_c}$  are explained simultaneously. Our result may also be used to predict the prompt  $J/\psi$  production and shed light on the  $J/\psi$  polarization puzzle.

We emphasize that in  $\chi_{cJ}$  production the NLO corrections already scale as  $1/p_T^4$ , which is the leading  $p_T$  behavior, and the NNLO and other corrections are no longer important, because they are suppressed either by  $\alpha_s$  or by  $v^2$  relative to NLO contributions. This differs markedly from  $J/\psi$  production, where NNLO corrections could be even more important than NLO at large  $p_T$  [20]. As a result, we have picked up the most important contributions in  $\chi_{cJ}$  production, and given a good description for this process. This work gives strong support to the color-octet mechanism, and provides further tests for NRQCD and heavy quakonium production mechanisms at the LHC.

We thank C. Meng and Y.J. Zhang for helpful discussions, and J. P. Lansberg, B. Gong and J.X. Wang for useful communications. This work was supported by the National Natural Science Foundation of China (No.11021092, No.11075002) and the Ministry of Science and Technology of China (No.2009CB825200).

- 
- [1] G. T. Bodwin, E. Braaten and G. P. Lepage, Phys. Rev. D **51**, 1125 (1995) [Erratum-ibid. D **55**, 5853 (1997)].
  - [2] N. Brambilla *et al.*, hep-ph/0412158; J. P. Lansberg, Int. J. Mod. Phys. A **21**, 3857 (2006); J. P. Lansberg *et al.*, arXiv:0807.3666.
  - [3] A. Abulencia *et al.* [CDF Collaboration], Phys. Rev. Lett. **98**, 232001 (2007).
  - [4] P. L. Cho and A. K. Leibovich, Phys. Rev. D **53**, 150 (1996).
  - [5] B. A. Kniehl, G. Kramer and C. P. Palisoc, Phys. Rev. D **68**, 114002 (2003).
  - [6] E. Braaten and J. Lee, Phys. Rev. D **67**, 054007 (2003); K. Y. Liu, Z. G. He and K. T. Chao, Phys. Lett. B **557**, 45(2003), Phys. Rev. D **77**, 014002 (2008); K. Hagiwara, E. Kou and C. F. Qiao, Phys. Lett. B **570**, 39 (2003).
  - [7] Y. J. Zhang, Y. J. Gao and K. T. Chao, Phys. Rev. Lett. **96**, 092001 (2006); Y. J. Zhang and K. T. Chao, Phys. Rev. Lett. **98**, 092003 (2007); B. Gong and J. X. Wang, Phys. Rev. D **77**, 054028 (2008); B. Gong and J. X. Wang, Phys. Rev. D **80**, 054015 (2009); Y. Q. Ma, Y. J. Zhang and K. T. Chao, Phys. Rev. Lett. **102**, 162002 (2009); B. Gong and J. X. Wang, Phys. Rev. Lett. **102**, 162003 (2009).
  - [8] P. Artoisenet, J. M. Campbell, F. Maltoni and F. Tramontano, Phys. Rev. Lett. **102**, 142001 (2009).
  - [9] C. H. Chang, R. Li and J. X. Wang, Phys. Rev. D **80**, 034020 (2009). M. Butenschoen and B. A. Kniehl, Phys. Rev. Lett. **104**, 072001 (2010);
  - [10] J. M. Campbell, F. Maltoni and F. Tramontano, Phys. Rev. Lett. **98**, 252002 (2007).
  - [11] B. Gong and J. X. Wang, Phys. Rev. Lett. **100**, 232001 (2008); Phys. Rev. D **78**, 074011 (2008).
  - [12] A. I. Davydychev, Phys. Lett. B **263**, 107 (1991).
  - [13] T. Hahn, Comput. Phys. Commun. **140**, 418 (2001).
  - [14] B. W. Harris and J. F. Owens, Phys. Rev. D **65**, 094032 (2002).
  - [15] R. K. Ellis and G. Zanderighi, JHEP **0802**, 002 (2008).
  - [16] T. Hahn and M. Perez-Victoria, Comput. Phys. Commun. **118**, 153 (1999).
  - [17] Y. Q. Ma, K. Wang and K. T. Chao, in preparation.
  - [18] M. R. Whalley, D. Bourilkov and R. C. Group, arXiv:hep-ph/0508110.
  - [19] E. J. Eichten and C. Quigg, Phys. Rev. D **52**, 1726 (1995).
  - [20] F. Abe *et al.* [CDF Collaboration], Phys. Rev. Lett. **79**, 578 (1997).
  - [21] P. Artoisenet, J. M. Campbell, J. P. Lansberg, F. Maltoni and F. Tramontano, Phys. Rev. Lett. **101**, 152001 (2008); J. P. Lansberg, Eur. Phys. J. C **61**, 693 (2009).